

Relationship between protein structural fluctuations and rebinding dynamics in ferric haem nitrosyls

Neil T. HUNT*, Gregory M. GREETHAM†, Michael TOWRIE†, Anthony W. PARKER† and Nicholas P. TUCKER‡¹

*Department of Physics, University of Strathclyde, Glasgow G4 0NG, Scotland, U.K., †STFC Rutherford Appleton Laboratory, Harwell Science and Innovation Campus, Didcot, Oxon OX11 0QX, U.K., and ‡Strathclyde Institute for Pharmaceutical and Biomedical Sciences, University of Strathclyde, 161 Cathedral Street, Glasgow G4 0RE, Scotland, U.K.

The interaction of nitric oxide (NO) with haem proteins is widespread in biology. In the current paper, we present the first ultrafast 2D-IR (two-dimensional infrared) spectroscopic analysis of haem nitrosylation, which has been combined with time-resolved IR pump–probe studies to investigate the relationship between equilibrium vibrational dynamics of the haem environment and ligand rebinding behaviour following photolysis of NO from the Fe(III)–NO site. Studies of two haem proteins, Mb (myoglobin) and Cc (cytochrome *c*), which play different physiological roles, reveal marked contrasts in the ultrafast fluctuations of the protein pockets containing the haem, showing that the Mb pocket is somewhat more flexible than that of Cc. This

correlates strongly with slower observed photolysis rebinding kinetics of Mb–NO compared with Cc–NO, and indicates a direct link between ultrafast fluctuations and biological functionality. Furthermore, this indicates the validity of linear response theories in relation to protein ligand binding. Finally, 2D-IR shows that Cc–NO displays two distinct structural sub-sites at room temperature that do not exchange on the timescales accessible via the NO vibrational lifetime.

Key words: biophysics, haem protein, two-dimensional infrared (2D-IR) spectroscopy, ultrafast spectroscopy.

INTRODUCTION

The structure of biological molecules defines their functionality and specificity. It is also clear that proteins are not static entities, but that they undergo changes in structure on a wide range of time and length scales. These changes may take the form of rapid fluctuations, which occur on the order of tens of femtoseconds (fs) to picoseconds (ps), or side-chain motions and secondary-structure changes that take place on nanosecond (ns) to millisecond (ms) timescales. Furthermore, the dynamic effects of hydrogen bonding add an extra layer of complexity. Despite a significant amount of work examining the interplay of structure, dynamics and reactivity, however, a clear picture of the role of ultrafast motions in determining protein behaviour has not been established.

Haem proteins have been the subject of much study as a result of their diverse roles in fundamental biological processes [1,2]. In particular, the dynamics of binding small molecules, such as O₂ and CO, and the behaviour of these systems following ligand photolysis have attracted significant interest, showing the rebinding kinetics to be a complex function of protein and haem group dynamics [3–10]. Ultrafast vibrational echo [11–13] and 2D-IR (two-dimensional infrared) spectroscopies have also emerged as effective probes of these systems [14–16]. The equilibrium fluctuations of a number of carboxyhaem proteins and their mutants have been investigated by exploiting the ability of the CO ligand to reflect the fluctuations of the haem pocket electrostatic environment due to the protein scaffold [17–20]. By determining the FFCF (frequency–frequency correlation functions) for the CO vibration in combination with molecular dynamics simulations, these studies have revealed protein dynamics on a range of timescales.

The NO (nitric oxide) radical is of fundamental importance in biology, participating in processes such as vasodilation, signalling

and immunity [21,22]. As a radical, NO is highly reactive with transition metals such as iron, via interactions with their *d*-orbitals [22]. Metalloproteins, such as those containing haem groups, are therefore particularly sensitive targets for the NO radical. This is particularly notable since some of the most fundamentally important proteins in the respiratory chain and TCA (tricarboxylic acid) cycle include NO-sensitive haem groups and iron–sulfur clusters [23,24]. Most organisms are able to sense NO and alter gene expression accordingly, allowing that organism to elicit a physiological response or to detoxify harmful quantities of NO [25,26]. To date, studies of the interactions of the NO ligand with haem proteins have concentrated largely on the ferrous form, facilitating useful comparisons with the carboxyhaem derivatives discussed above. Unlike CO and O₂, however, NO binds to ferric haem centres, but studies of such systems are generally restricted to rebinding studies of the NO ligand using FTIR (Fourier-transform infrared) [9] or visible light spectroscopy [8]. An exception to this is the nitrophorins [27], which naturally function in the ferric form and which have also been investigated using ultrafast coherence and Raman methods [28], but there exist no studies applying ultrafast IR or 2D-IR methods to study ferric nitrosylated haem proteins.

In the present study, we employ ultrafast 2D-IR spectroscopy to probe the vibrational dynamics of the Fe(III)–NO site, and provide insights into the fluctuations of the haem pocket environment of two proteins, Mb (myoglobin) and Cc (cytochrome *c*). These equilibrium dynamics are compared with the non-equilibrium behaviour of the NO ligand following photolysis from the haem centre, allowing the relationships between protein flexibility and rebinding dynamics to be observed. The strong correlation observed indicates a link between ultrafast dynamics and functionality, and establish the validity of linear response theories for ligand binding.

Abbreviations used: Cc, cytochrome *c*; 2D-IR, two-dimensional infrared; FFCF, frequency–frequency correlation function; FTIR, Fourier-transform infrared; Mb, myoglobin; OPA, optical parametric amplifier; TRIR, time-resolved IR.

¹ To whom correspondence should be addressed (email nick.tucker@strath.ac.uk).

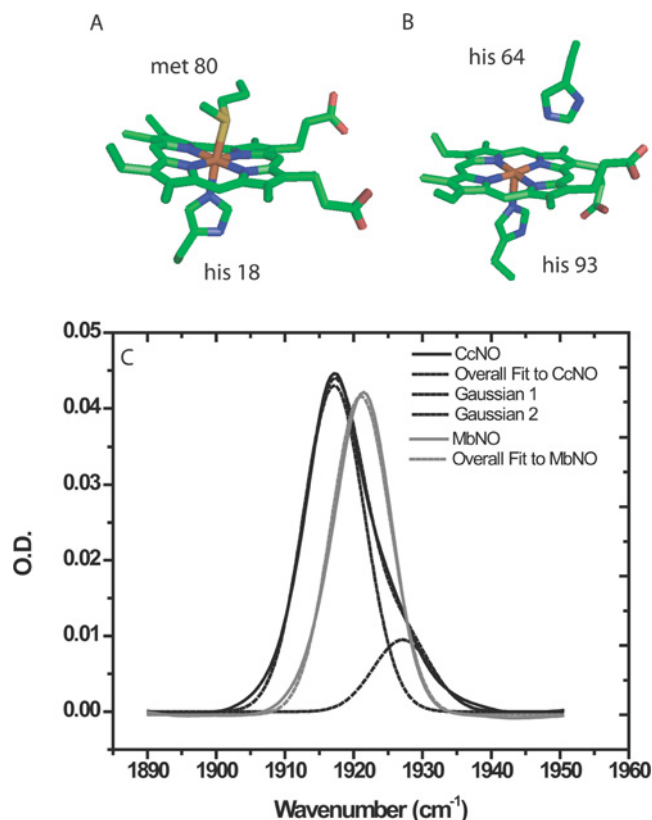


Figure 1 Haem co-ordination and FTIR spectra of nitrosylated Cc and Mb

Co-ordination of the haem groups of equine (A) Cc (PDB code 1HRC [31]) and (B) Mb (PDB code 1YMB [30]) demonstrating the structural differences of distal ligands to the ferric haem centre. (C) FTIR spectra of ferric Cc–NO (black) and Mb–NO (grey) near 1900 cm^{-1} . Solid lines show background-subtracted experimental data, and the broken lines show the results of fitting to Gaussian lineshape functions (see the text for details).

Ferric Mb is rare in healthy muscle tissue where it is reduced to the ferrous form which is capable of the reversible binding of oxygen that defines its primary function. It is, however, thought to be generated via the detoxification of NO to nitrate by oxymyoglobin [1]. Cc is a redox-active protein that must be in its ferric state in order to receive electrons from ubiquinol Cc-reductase (complex III) prior to transfer to Cc-oxidase (complex IV). Cc does not bind molecular oxygen as Mb does, but both proteins can accommodate NO at their haem groups [2]. As these proteins play very different physiological roles, with Mb acting as a ligand reservoir, and Cc is involved in electron-transfer processes, a comparative study enables insights into the possible influence of ultrafast pocket dynamics on biological functionality.

The haem pockets of Mb and Cc are structurally well characterized: the Mb haem exists in a five-co-ordinate geometry in the deoxy state, with proximal co-ordination of the iron via the His⁹³ residue [29,30], leaving a vacant distal site for diatomic ligand binding. The sixth co-ordination site can also be occupied by a water molecule, although this is competitively displaced by diatomic ligands of the types discussed above. By contrast, in the absence of exogenous ligands, the Cc distal site is co-ordinated by a sulfur atom from the distal Met⁸⁰ residue, and the proximal site is co-ordinated by the His¹⁸ residue, leading to a hexa-co-ordinated haem moiety [31] (Figures 1A and 1B). In the presence of NO, the distal residue co-ordination is replaced by the diatomic ligand [32].

EXPERIMENTAL

Preparation of proteins

Freeze-dried equine heart Mb or Cc (Sigma) were resolubilized (50 mg/ml) in deuterated phosphate buffer (pH 7.0) and Noc-9 (MAHMA NONOate; Sigma) was added to a 3-fold molar excess to nitrosylate the protein. No significant quantities of insoluble protein were observed in the samples. The fact that the IR vibrational mode specific to the ferric haem nitrosyl NO stretching vibration was employed as a probe for all spectroscopic experiments guards against problems due to the presence of small quantities of oxyMb. Both proteins are known to undergo reductive nitrosylation, but the timescales for this were observed to be long in comparison with those for data collection. To confirm this, the FTIR spectrum of the sample was obtained pre- and post-laser experiments.

Ultrafast spectroscopy

The experiments were carried out using the ULTRA spectrometer (<http://www.clf.stfc.ac.uk/Facilities/Lasers+for+Science+Facility/Molecular+Structure+and+Dynamics/12264.aspx>) and the methodology employed has been described previously [33]. Briefly, the tunable IR pump ($\sim 10 \text{ cm}^{-1}$ bandwidth) and probe (400 cm^{-1} bandwidth) pulses used for double-resonance 2D-IR spectroscopy were generated by two OPAs (optical parametric amplifiers) pumped by synchronized Ti:sapphire-based regenerative amplifiers with ps and fs pulse duration respectively. Both OPAs used difference frequency mixing of the signal and idler beams to generate the mid-IR wavelength pulses. For 2D-IR spectra acquisition, the pump frequency was scanned across the region of interest for a fixed pump–probe time delay and the probe spectrum recorded via a HgCdTe array detector and spectrometer combination that yielded a spectral resolution of 2 cm^{-1} . The pump pulse trains were chopped at half the laser repetition rate (10 kHz) to facilitate collection of $\text{IR}_{\text{pump on}} - \text{IR}_{\text{pump off}}$ difference spectra, and optical delay lines controlled relative pulse timings. The pump–probe polarization relationships were set to the magic angle to remove the effects of molecular rotation in all experiments, except those to determine the IR anisotropy, which employed alternating parallel and perpendicular polarization geometries. In all experiments the pump pulse intensities were reduced to prevent line broadening effects. Examples of slices through the 2D-IR spectra obtained in this manner showing the sensitivities and signal-to-noise ratios obtained are presented in Figure 3.

For time-resolved infrared ($\text{UV}_{\text{pump}} - \text{IR}_{\text{probe}}$) experiments, the methodology was similar, but a third OPA produced the necessary 350 nm wavelength UV_{pump} pulses via fourth harmonic generation. The samples were held between two CaF_2 windows separated by a PTFE [poly(tetrafluoroethylene)] spacer with a thickness of $100 \mu\text{m}$. For TRIR (time-resolved IR) measurements, the sample was flowed in order to refresh the probed volume.

RESULTS

The FTIR spectra of ferric Mb–NO and Cc–NO (Figure 1) both display a peak near 1920 cm^{-1} . The Cc–NO spectrum was also observed to feature a shoulder on the blue edge of the main band. Haem-nitrosylation is well-established under these conditions and the peaks are assigned to N–O stretching modes of the Fe(III)–NO complex [9,10]. Fitting the spectra to Gaussian lineshape functions revealed that, for Mb–NO, the spectrum was well-represented by a single function, centred at 1921.0 cm^{-1} with a width of $\sim 10 \text{ cm}^{-1}$, and for Cc–NO two lineshapes were required

Table 1 Results of fitting 2D-IR and TRIR data (see the text for details)

Experiment	Unit	Cc-NO		Mb-NO
		A ₁	A ₂	
FTIR				
a _{gauss} (amplitude)		0.043	0.010	0.041
$\bar{\nu}$ _{gauss} (frequency)	cm ⁻¹	1917.2	1927.1	1921.0
σ _{gauss} (width)	cm ⁻¹	10.44	10.02	10.12
Spectral diffusion				
α_1 (amplitude)		0.22	–	0.29
τ (decay time)	ps	12.3	–	5.8
α_2 (constant term)		0.27	–	0.15
Vibrational relaxation				
A _{vib} ($\nu = 1-2$) (amplitude)		0.030 (0.025)	0.002 (0.002)	0.015 (0.013)
T ₁ ($\nu = 1-2$) (decay time)	ps	23.7 (23.3)	18.6 (18.1)	22.5 (22.5)
Rebinding dynamics (bleach)				
A _{rebind} (amplitude)		1.6×10^{-3}	–	1.4×10^{-4}
τ _{rebind} (rebinding / recovery time)	ps	12.7	–	32.4
A _{static} (static amplitude)		1.5×10^{-4}	–	4×10^{-5}
Photoproduct dynamics				
A _{rise} (rise coefficient)		-4×10^{-5}	-4×10^{-5}	–
τ _{rise} (rise time)	ps	2.5	2.5	–
A _{decay} (decay coefficient)		1×10^{-4}	1×10^{-4}	–
τ _{decay} (decay time)	ps	36	36	–
A _{static} (static amplitude)		0	0	–

to achieve a similar quality of fit. In this case, both functions featured a width of ~ 10 cm⁻¹ and were centred at 1917.2 and 1927.1 cm⁻¹ respectively. The quantitative fitting results are shown in the FTIR section of Table 1, where a_{gauss}, $\bar{\nu}$ _{gauss} and σ _{gauss} represent amplitude, frequency and width parameters respectively and the functions are compared with the spectra in Figure 1 (broken lines). These results suggest that the ferric Cc-NO species exists in two subsites, a situation that has been observed for Mb-CO and its mutants, but has not been reported for ferric Cc-NO [19]. Temperature-dependence measurements of the FTIR spectrum of Cc-NO were carried out, but no substantial changes in the lineshapes or evidence of coalescence were observed up to 333 K. In the remaining discussion, we will refer to these subsites of Cc-NO as A₁ (main peak, 1917.2 cm⁻¹) and A₂ (shoulder, 1927.1 cm⁻¹).

Figures 2(a) and 2(c) show ultrafast 2D-IR spectra of Cc-NO at two pump-probe time delays. The spectra show a clear negative peak located on the spectrum diagonal at (probe, pump) = (1917, 1917) corresponding to the bleach and stimulated emission of the A₁ site $\nu = 0-1$ transition, along with a positive peak located at (1889, 1917) assignable to the transient absorption arising from the $\nu = 1-2$ transition. The latter is shifted along the probe axis by 28 cm⁻¹ due to the anharmonicity of the vibrational mode. It is also possible to detect the presence of a much weaker peak pair at (1927, 1927) and (1897, 1927) that are attributable to the corresponding transitions of the A₂ subsite, but these are dominated in the two-dimensional spectrum by the main A₁-derived peaks. The presence of these contributions to the 2D-IR spectra are shown more clearly in Figure 3 using slices through the 2D-IR spectrum taken at a range of pump frequencies for a fixed pump-probe time delay. Figure 3(A) shows slices recorded for pump frequencies to the low-frequency side of the centre of the A₁ NO stretching mode, whereas Figure 3(B) shows those for higher pump frequencies. In the latter spectra the presence of a second mode in both the positive ($\nu = 1-2$) and negative ($\nu = 0-1$) contributions to the spectrum are clearly observed and these are highlighted by arrows in the Figure. This is as would be expected because the A₂ band would only be expected to be present in the slices when the pump frequencies coincided with the

spectral envelope of this mode. At the highest pump frequencies, the A₂ contribution, although small, is clearly seen to dominate the lineshape. The anharmonic shift of this mode is almost identical with that of the A₁ subsite.

Figures 4(a) and 4(c) show the corresponding 2D-IR spectra for Mb-NO. These consist of a single pair of peaks located near (1921, 1921) and (1893, 1921) which are attributable to the $\nu = 0-1$ and $1-2$ transitions of the N-O stretching mode of the Mb-NO complex respectively. The effects of anharmonicity are comparable with those observed in the Cc-NO spectra.

In the 2D-IR spectra of Cc-NO and Mb-NO, the lineshapes evolve as a function of pump-probe time delay. This can be perceived in Figures 2 and 4 either as a loss of the diagonal elongation that is present at short pump-probe time delays or as a rotation of the nodal plane between the two components ($\nu = 0-1$ and $\nu = 1-2$) of the 2D-IR lineshape towards the vertical as the pump-probe time delay increases. This process has been described extensively and is attributed to spectral diffusion of the inhomogeneously broadened NO vibrational mode [34,35]. Inhomogeneous broadening is caused by changes in the electrostatic environment of the NO ligand as the protein pocket fluctuates, which are manifest in the NO stretching frequency via a Stark shift of the absorption band. As a result, each NO probe in an ensemble will experience a slightly different environment and thus a slightly different stretching frequency. It has been shown via Stark spectroscopy that the NO stretching frequency provides a sensitive probe of the electrostatic interaction of the protein scaffold with the NO group [36]. Thus if the protein pocket fluctuations are slow on the timescale of the measurement, then a temporal evolution of the 2D-IR lineshape is expected as the NO probes sample each of the environments that contribute to the complete absorption band. When quantified, the temporal evolution of this spectral diffusion provides a measurement of the FFCF, which describes the amplitude and timescale of the ultrafast fluctuations occurring in the haem pocket.

The 2D-IR lineshapes of Mb-NO and Cc-NO obtained at pump-probe delay times from 5 to 50 ps were fitted to a two-dimensional Gaussian function of the form (eqn 1):

$$\sum_i A_i \exp \left[- \frac{1}{2(1-c_{2D,i}^2)} \left[\left(\frac{x-x_{0,i}}{\sigma_{x,i}} \right)^2 + \left(\frac{y-y_{0,i}}{\sigma_{y,i}} \right)^2 - \frac{2c_{2D,i}(x-x_{0,i})(y-y_{0,i})}{\sigma_{x,i}\sigma_{y,i}} \right] \right] \quad (1)$$

where A represents the amplitude, x_0 and y_0 are the peak coordinates (x represents the probe axis) and σ_x and σ_y are the corresponding width parameters. The cross-correlation parameter, c_{2D} , which ranges from -1 to 1 , provides a measurement of the diagonal elongation of the lineshape. In the case of c_{2D} , a value of 1 indicates a strongly correlated lineshape elongated along the diagonal of the 2D-IR spectrum. If c_{2D} is zero, the line will be uncorrelated and circular in shape. Finally, a c_{2D} value of -1 indicates an anticorrelated lineshape, which will be elongated along the antidiagonal of the spectrum.

For an inhomogeneously broadened lineshape, such as that observed in Figures 2 and 4, the value of c_{2D} would be expected to vary from a positive value towards 0 as the time delay increases due to the NO ligand sampling the different environments created by the haem pocket through protein fluctuation. Quantification of the temporal variation of the c_{2D} parameter provides the FFCF.

It is noted that the fitting process was started at a pump-probe delay time of 5 ps to avoid coherent contributions to the data

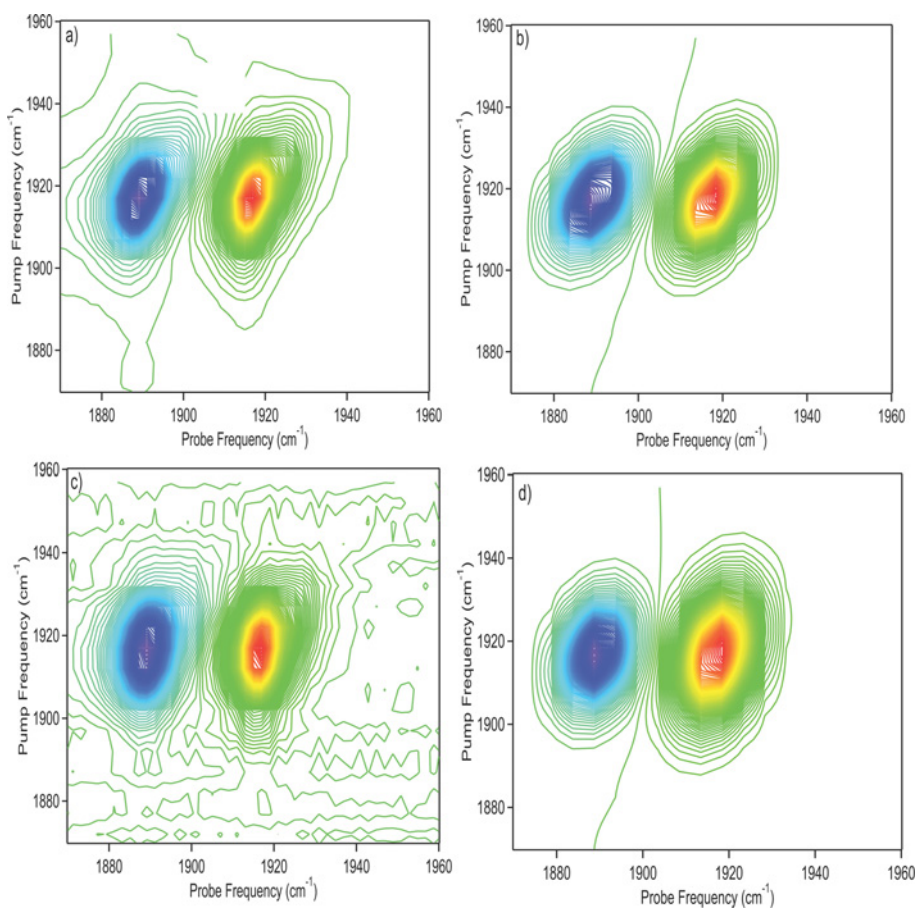


Figure 2 2D-IR spectra of nitrosylated Cc

2D-IR spectra of Cc-NO recorded with a time delay of (a) 5 ps and (c) 50 ps. (b) and (d) are fits to the data in (a) and (c) respectively using a two-dimensional Gaussian function (see the text for details). Contour colour scale runs from red (negative) to blue (positive).

caused by temporal overlap of the narrow bandwidth pump pulse with the probe pulse. Fits to the 2D-IR spectra in Figures 2 and 4 are shown in (b) and (d) and the temporal variation of c_{2D} is displayed in Figure 5(A). As the $\nu = 0-1$ and $\nu = 1-2$ components of the lineshape will be expected to show identical dynamics, the c_{2D} parameters obtained for each were averaged to provide the data shown in Figure 5(A); the error bars in this Figure indicate the repeatability of the data. The lineshape evolution was also analysed using other established metrics [35,37,38], which have been shown to yield quantitative measurements of the FFCF, and the dynamics obtained were in excellent agreement with the variation of the c_{2D} parameter. Although the Cc-NO spectra consist of overlapping lineshapes from two subsites, the two-dimensional spectrum was dominated by the A_1 transitions to such an extent that distortion of the fit by the presence of the shoulder was minimal. This was confirmed by the close agreement of the data derived from the c_{2D} parameter and the nodal line slope method [35,38] for the A_1 transitions. The latter uses the rotation of the nodal plane between the two halves of the 2D-IR lineshape to quantify the lineshape evolution and so will be unaffected by the presence of the second transition.

Three observations can be made based upon the data in Figure 5(A). First, for both proteins, the value of c_{2D} is less than unity at zero pump-probe time delay. This suggests that some of the processes causing spectral diffusion occur on timescales shorter than the 1–2 ps time-resolution of the technique, giving rise to this

otionally narrowed contribution. Secondly, a decay timescale of a few ps is observed for both proteins, and thirdly the c_{2D} value does not fall to zero, implying that there are slow, pseudostatic processes that lead to spectral diffusion on timescales longer than 50 ps. As the measurement is constrained by the vibrational lifetime of the NO ligand (see below), the dynamics of these processes are inaccessible via this experimental methodology.

The data in Figure 5(A) were fitted to the sum of a single exponential decay and a constant term of the form (eqn 2):

$$c_{2D} = \alpha_1 \exp\left[\frac{-t}{\tau}\right] + \alpha_2 \quad (2)$$

where α_1 and τ represent the amplitude and decay time of the exponential function and α_2 is a constant term; effectively the amplitude of a second decay profile with an infinite decay time. This equation represents a measurement of the FFCF for the NO vibrational mode. The fitting yielded the parameters shown in the spectral diffusion section of Table 1. Based upon the fact that the decay time (τ) is approx. 5.8 ps for Mb but 12.3 ps for Cc, the results imply that the protein pocket of Mb is significantly more flexible than that of Cc. The non-decaying part of the fit is smaller in amplitude for Mb than Cc, showing that a larger fraction of the possible conformations are sampled during the experimental time window, which is also consistent with increased flexibility.

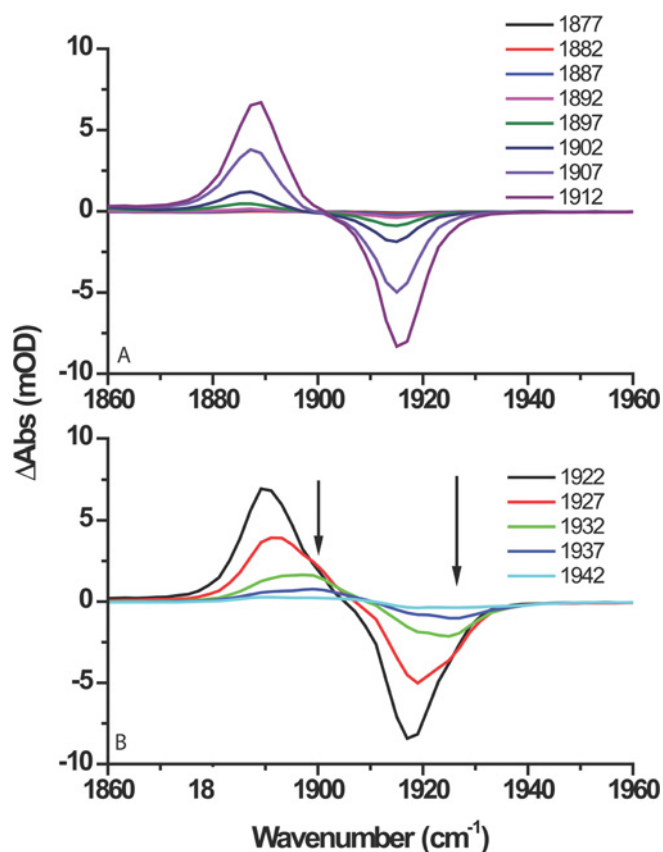


Figure 3 Slices through 2D-IR spectra of Cc-NO

Spectra were recorded with a pump-probe delay time of 5 ps. **(A)** Slices corresponding to pump wavelengths on the red side of the main NO stretching transition, whereas **(B)** shows slices recorded with higher pump frequencies. The key reports pump frequencies in cm^{-1} . The contributions from the A_2 state are clearly observed in **(B)** and are marked with arrows.

The vibrational lifetime of the NO stretching mode, the time over which the excited state decays, was obtained from the 2D-IR data and the results for the Cc-NO A_1 state are shown in Figure 5(B). The Figure shows the decay of the signal from the $\nu = 0-1$ and $1-2$ transitions which were well-represented by a single exponential function (solid lines) of the form (eqn 3):

$$\text{Peak amplitude} = A_{\text{vib}} \exp\left[\frac{-t}{T_1}\right] \quad (3)$$

with a decay time or vibrational lifetime, T_1 , of approx. 23 ps (see the vibrational relaxation section of Table 1, where A_{vib} represents the amplitude of the decay function). The results for Mb-NO revealed a very similar vibrational lifetime to this state of Cc-NO. Interestingly, the A_2 state of Cc-NO revealed a somewhat shorter lifetime of 18.5 ps (see Table 1). The dominance of the two-dimensional signal by the A_1 transition made fitting to two two-dimensional Gaussians inconclusive, but the two signals were separated using fits of slices (Figure 3) through the 2D-IR data at a pump frequency of 1930 cm^{-1} to one-dimensional Gaussian lineshapes. It is important to stress that no evidence of cross peaks linking the A_1 and A_2 modes were observed, except as a result of pumping the strong A_1 mode with the wings of the pump pulse bandwidth when the pump frequency was centred on the A_2 mode. The reverse peak was not resolved as a result of the relatively low intensity of the A_2 transition. The lack of these

cross peaks implies that the two subsites are not exchanging on the timescale of the experiment.

Using 2D-IR signals obtained using parallel (R_{para}) and perpendicular (R_{perp}) pump-probe polarization geometries, the rotational relaxation time of the NO (which acts as a probe for the protein) was recovered via the anisotropy decay. The anisotropy parameter is derived from the relationship (eqn 4):

$$R_{\text{aniso}} = (R_{\text{para}} - R_{\text{perp}})/(R_{\text{para}} + 2R_{\text{perp}}) \quad (4)$$

In order to verify the accuracy of the polarization settings, the magic angle data used for vibrational relaxation measurements were recreated using the relation $R_{\text{MA}} = R_{\text{para}} + 2R_{\text{perp}}$, which showed excellent agreement. The temporal dependence of the anisotropy for Cc-NO and Mb-NO were very similar, revealing that the anisotropy of the NO mode undergoes no decay attributable to rotational reorientation, indicating that this process is slow on these timescales, as anticipated for a large protein.

To complement these equilibrium dynamics studies, the behaviour of the Mb-NO and Cc-NO systems following UV photolysis of the NO ligand were determined. The results of the transient IR measurements (Figure 6) show clear differences between the two proteins. For Cc-NO, photolysis resulted in a bleach of the A_1 and A_2 subsites (Figure 6a), with no differentiation between them possible in the observed data either in terms of fractional bleach or recovery rate; no time evolution of the bleach lineshape was observed other than a decrease in amplitude. The dynamics of the recovery (Figure 6b, black squares) were well-represented by an exponential decay function of the form (eqn 5):

$$\text{Peak amplitude} = A_{\text{rebind}} \exp\left[\frac{-t}{\tau_{\text{rebind}}}\right] + A_{\text{static}} \quad (5)$$

where A_{rebind} is the amplitude coefficient and τ_{rebind} the timescale for rebinding/recovery respectively; A_{static} is the amplitude coefficient of the static component, this corresponds with the fraction of NO molecules that do not rebind to the haem within the experimental timescale.

The results of the fitting are displayed in the rebinding dynamics (bleach) section of Table 1. For Cc-NO the bleach recovered with a timescale of 12.7 ps (τ_{rebind}) and a static component (A_{static}) of $\sim 10\%$ of the initial bleach. Also visible in Figure 6(a) is a small photoproduct peak near 1830 cm^{-1} . Fitting the dynamics of this peak to a bi-exponential function very similar to eqn (5), but with two exponential terms with parameters A_{rise} (amplitude) and τ_{rise} (timescale) included to fit the rising portion of the data, A_{decay} (amplitude) and τ_{decay} (timescale) to fit the decay alongside a static amplitude term A_{static} . This approach gave a rise time (τ_{rise}) of 2.5 ps followed by a 36 ps decay (τ_{decay}) (see Table 1, photoproduct dynamics). In the case of the photoproduct, no signal remained at long times, ($A_{\text{static}} = 0$) suggesting a transient nature, although it is clear that the ground state recovery is likely to be only partially due to direct transfer from the photoproduct given the difference in timescales. The small amplitude of this photoproduct band indicates either a low concentration or a weak transition dipole moment, but no significant 36 ps timescale was observed in the bleach recovery.

For Mb-NO photolysis, the recovery timescale for the Mb-NO bleach (Table 1) was also fitted to a single exponential function with a static contribution, giving a recovery timescale of 32 ps and a static amplitude of approx. 30% of the initial bleach. The initial bleach was an order of magnitude smaller than that obtained for Cc-NO and no photoproduct bands were observed. The data for Mb-NO compare well with FTIR studies of ferric

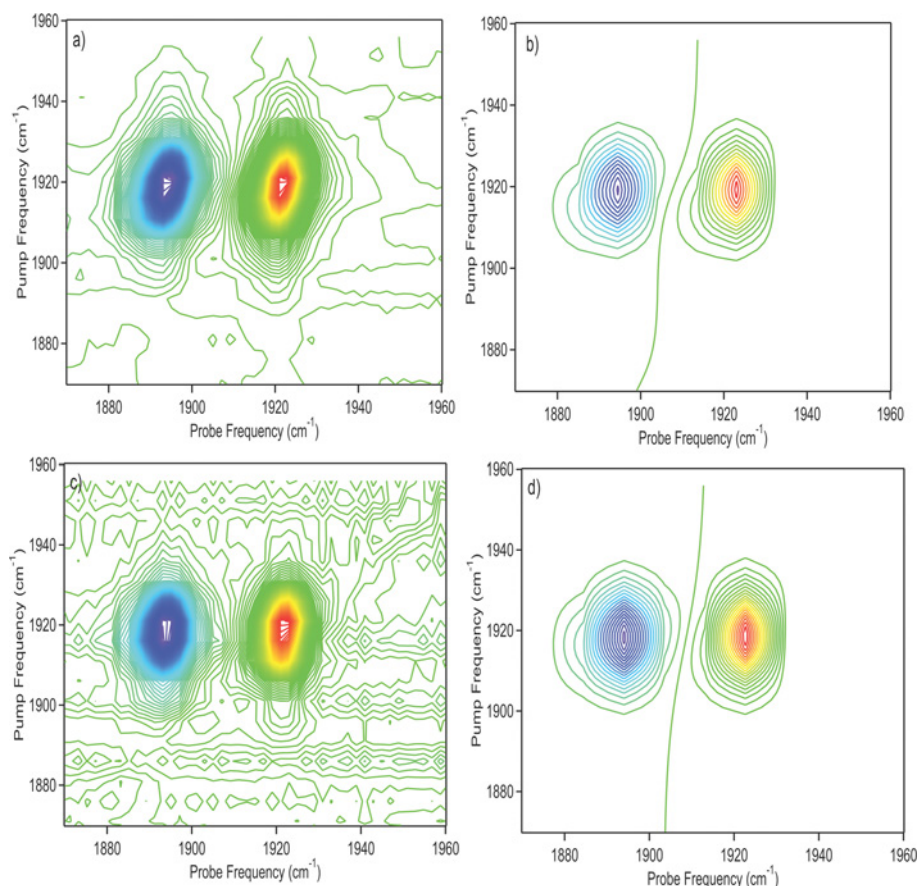


Figure 4 2D-IR spectra of nitrosylated Mb

2D-IR spectra of Mb-NO recorded a time delay of (a) 5 ps and (c) 50 ps. (b) and (d) are fits to the data in (a) and (c) respectively using a 2D Gaussian function (see the text for details). Contour colour scale runs from red (negative) to blue (positive).

Mb-NO rebinding, which also indicated a reduced quantum yield in comparison with ferrous Mb-NO and an absence of photoproduct absorptions for Fe(III)-Mb-NO [9].

DISCUSSION

It is clear that the role of the protein structure will be pivotal in determining the observed dynamics. In the NO-bound state, both proteins feature a hexa-co-ordinate Fe(III) centre and a proximally bound histidine residue. In the case of Mb, the distal ligand that is in closest proximity to the NO, and so most likely to participate in any direct protein side chain-ligand interactions, is the His⁶⁴ residue (Figure 1B), whereas in Cc the equivalent interaction will be via a methionine side chain (Met⁸⁰) (Figure 1A). In Cc, two cysteine residues (Cys¹⁴ and Cys¹⁷) also bind to the porphyrin ring of the haem group, which may enhance the structural stiffness.

When discussing dynamics, it is also important to consider the binding of the NO to the iron centre. In the ferric form, the Fe(II)-NO(+) description of the ground state [9,39,40] has been shown to be most appropriate, which leads to a ground state that is isoelectronic with that of Fe(II)-CO. The interaction between ligand and the metal centre incorporates back-electron donation between the Fe and the N atoms that causes an anticorrelation between the Fe-N and N-O bond strengths and vibrational frequencies. This description also implies a slight positive charge

on the NO ligand, which may facilitate interaction with accessible electron lone pairs from nearby distal side chains such as His⁶⁴ in the case of Mb (Figure 1B) [9,40].

Considering the equilibrium dynamics of both proteins, these are broadly similar in that both feature a fast, motionally narrowed component followed by a ps timescale decay and a static component that is too slow to be observed via these experiments. Clear differences also occur, however, in particular, the FFCF-related parameters obtained for Mb-NO (Figure 5a) are smaller in value than those of Cc-NO, whereas the ps decay of the function is faster than that of Cc-NO. These point to a higher spectral diffusion rate for the NO ligand in Mb compared with Cc, and thus a more flexible haem pocket environment in Mb.

Comparison of these data with similar studies on wild-type ferrous Mb-CO reveals similarities, as expected if the protein scaffold is the significant contributor to the observed dynamics. In particular, a 4.95 ps decay timescale was reported for wild-type Mb-CO alongside a static contribution [11-13]. Similar studies of a ferrous carboxy Cc mutant revealed an 8 ps decay time for the FFCF [41], again in good agreement with the parameters observed in the present study for the ferric nitroso forms of Cc. This implies a relative insensitivity of the equilibrium protein dynamics to the oxidation state and ligand identity. 2D-IR investigations of carboxyneuroglobin (Ngb) and mutant Mb-CO proteins [19] revealed evidence of motionally narrowed processes alongside a bi-exponential decay with 2 and 14 ps

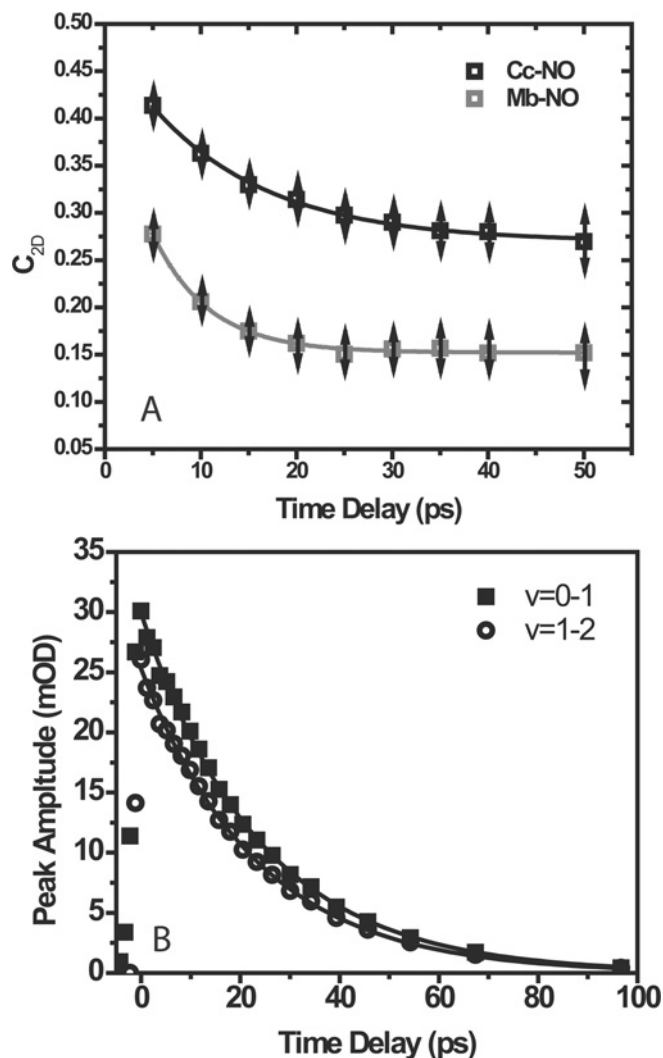


Figure 5 FFCF and vibrational dynamics of nitrosylated proteins

(A) Variation of cross-correlation parameter C_{2D} as a function of pump-probe delay time for Cc-NO (black lines) and Mb-NO (grey lines). Solid lines show a fit to exponential functions (see the text for details). (B) Vibrational relaxation for Cc-NO. Solid lines represent fits to single exponential decay functions (see the text for details).

timescales and a static component for one subsite (N_3), and an 11.5 ps exponential decay with a static component for a second subsite (N_0). The observation of dynamics in the 11–14 ps region indicates similarities with the Cc dynamics observed here. The time resolution of our 2D-IR measurements will result in the faster decay contributions being absorbed into the motionally narrowed dynamical component. In the case of the H64V mutant of MbCO, the CO stretching mode revealed FFCF dynamics on the 5.2 ps timescale [19], which is very close to the value observed for the ferric NO-ligated haem studied here. The H64V mutant lacks any interaction between the distal histidine residue and the ligand, so similarity with wild-type Mb-NO may indicate that this residue has little effect on the overall electrostatic fluctuations of the pocket or that effects of the change to the ferric form and the loss of this interaction cancel each other out. However, the L29F mutant of ferrous Mb, which will maintain the distal histidine interaction, showed a much faster decay profile with 1.7 and 66 ps components [19], indicating that the effects of mutations are

likely to be significant. It is highly unlikely, however, that a single residue will be solely responsible for the dynamics observed.

The observation of a somewhat stiffer protein scaffold in Cc is consistent with NMR studies [42]. As 2D-IR methods are able to access significantly shorter timescale dynamics than these methods, this suggests the existence of a link between the ultrafast dynamics and the longer timescale processes occurring in a given protein.

The origins of the fluctuations that give rise to these FFCFs are not clear. A Fourier transform relationship exists between the FFCF and the density of vibrational states that contribute to the fluctuations. However, the forms of the FFCF observed in Figure 5(A) suggest that the motions will be of very low (THz) frequency and broad bandwidth. This indicates that, rather than assigning the motions to a single mode or specific group of modes, they must be ascribed to the wide range of collective low-frequency librations of protein side chains or backbone motions that arise from the many degrees of freedom existing in a protein structure. In terms of haem group involvement, no specific evidence for interactions with vibrational modes of the haem are observed, in agreement with previous studies that suggest that haem group motions do not contribute significantly to electric field fluctuations on short timescales [11–13].

The structural environment of the NO ligand in these two proteins is interesting, particularly when compared with previous studies on the ferrous carboxy forms. In particular, three binding subsites are observed for Mb(II)-CO depending on the temperature [11–13], and these have been assigned to different positions of the His⁶⁴ residue side chain in relation to the CO ligand. These were not observed for Fe(III)-NO Mb, which showed no evidence for the presence of such subsites in the FTIR spectrum (Figure 1). It has been suggested that the ferric Mb-NO structure includes an interaction between the non-protonated form of the His⁶⁴ side chain and the NO ligand [9,40]. The results of the present study cannot confirm this interaction, except to indicate the presence of only one structural form at room temperature.

In the case of Cc-NO, a second subsite (A_2) was observed and it is possible to speculate on the structural basis for this. This site shows two main differences to the main A_1 site in the slightly higher transition frequency and a faster T_1 vibrational relaxation time. The higher vibrational frequency of the A_2 mode implies an increased interaction between the ligand and the protein backbone. This interaction must directly affect the vibrational frequency of the NO ligand, thus an interaction between the NO and the side chains of residues forming the haem pocket are more likely than one between the protein and the haem group. The closest distal ligand is the Met⁸⁰ residue, which in principle may interact with the NO via the S atom [40]. Such an interaction would disrupt the backbonding effect between the Fe and the N, leading to a weakened Fe-N bond and a slight strengthening of the N-O interaction and increased NO stretching frequency. A secondary effect of this interaction with the protein scaffold would be a faster T_1 relaxation. The contact between the ligand and the side chain would provide an alternative pathway for vibrational energy dissipation into the environment, reducing the observed T_1 value.

In the case of Cc-NO, no exchange was observed between the two subsites; this is in contrast with observations on Mb-CO mutants, which reported an exchange time of ~ 50 ps between subsites [17]. The increased stiffness of the Cc pocket would be consistent with a longer exchange time, and the lack of temperature dependence of the FTIR spectra reported above also implies a larger barrier to interconversion for Cc-NO.

Non-equilibrium, ligand rebinding studies of Mb-NO and Cc-NO reveal that both proteins show broadly similar dynamics, with

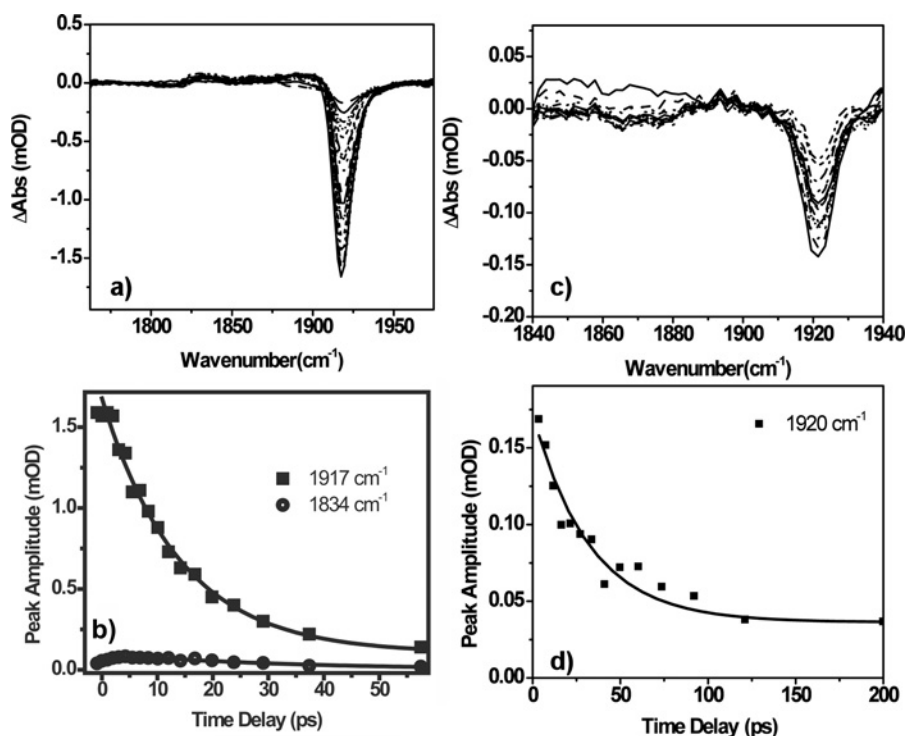


Figure 6 Transient IR spectroscopy data for NO photolysis from Cc-NO (a and b) and Mb-NO (c and d)

Fits to exponential decay functions in (b) and (c) are shown as solid lines.

rebinding characterized by a single exponential bleach recovery time. However, the relative timescales are significantly different, with Cc-NO showing a rebinding time that is twice as short as that of Mb-NO, whereas approximately three times as much NO escapes the Mb haem pocket following photolysis as does from Cc-NO. In addition, Cc-NO shows clear evidence of a photoproduct-binding site for the NO, whereas Mb-NO does not. The photoproduct site observed for Cc-NO following photolysis displays a frequency that is similar to those observed for ferrous Mb-NO and that of free NO [43], implying that this species involves NO located in a void in the protein pocket, possibly via hydrogen bonding or dipolar interactions. These sites are likely to be the 'Xenon pockets' that serve as binding sites for CO following photolysis [44].

The reason for the lower quantum yield for NO photolysis from Mb is unclear. It is possible that the presence of the nearby His⁶⁴ residue may play a role in restricting initial migration of the NO ligand that is not matched by the Cc-NO Met⁸⁰ residue. The fact that the Met⁸⁰ residue co-ordinates the haem iron while the Mb His⁶⁴ does not would suggest that this may be an unlikely explanation if mere proximity is the key factor. However, as the histidine interaction will be through a nitrogen rather than sulfur atom, the distal ligand effect may be expected to be stronger for Mb than Cc. Indeed, a stronger distal ligand interaction in Mb-NO than in Cc-NO may explain the single binding geometry observed for Mb and indicate a His⁶⁴ contact in this form, whereas the weaker Met⁸⁰ interaction in Cc-NO results in an equilibrium between subsites with (A₂) and without (A₁) distal side chain interaction. A similar quantum yield was observed for the H64L mutant via FTIR methods [9], and it is interesting to note that once the NO ligand has left the binding site, any increased distal ligand attraction plays no role in speeding up the rebinding dynamics, suggesting that this situation is rather complex.

The fact that the dynamics obtained for NO rebinding were described by single exponential functions for both ferric haem proteins is consistent with a study of ferric HRP (horseradish peroxidase), which also reported a single exponential decay profile for geminate NO rebinding [8]. Rebinding studies of the ferric nitrophorins reported bi-exponential dynamics, but these were attributed to closed and open states of the protein. For the closed state, the rebinding time of 15 ps is comparable with that of Cc, whereas the open form displayed rebinding dynamics an order of magnitude slower [27]. The rebinding dynamics of ferrous Mb-NO, which display multi-exponential characteristics, are significantly more complex than those observed for the ferric form [7]. This indicates that the chemical nature of the Fe-haem centre has a role to play in rebinding processes, but not in determining the equilibrium fluctuations of the pocket.

Considering the equilibrium and non-equilibrium studies together shows that the ligand rebinding time for Mb is ~2.5-fold slower than for Cc. This correlates extremely well with the relationship between the spectral diffusion timescales, which shows a factor of 2.1 faster relaxation for Mb compared with Cc. Taken together, these observations strongly suggest a relationship between pocket stiffness and rebinding dynamics and relate well to the increased percentage of the NO that escapes the pocket, or takes longer than the experimental timescale to rebound, in Mb compared with Cc. It has been speculated that the rebinding timescale for a photolysed ligand group is directly related to the volume of the protein pocket [5], this cannot be ruled out through the results of the present study as these also strongly suggest that the dynamics of the protein environment play a significant role.

Such a correlation between the equilibrium dynamics and recovery from a perturbed or non-equilibrium state is an important result. Furthermore, it is consistent with the predictions of linear

response and fluctuation–dissipation theories [45–47]. These state that the response of a system to a perturbation should be identical with the response to a small spontaneous fluctuation about the equilibrium state. The direct correlation between ligand rebinding time and the equilibrium fluctuations observed for these proteins would seem to indicate that these theories apply to protein ligand binding as well as to solute–solvent systems. The exact mechanism by which the fluctuations affect the propensity for ligand binding is unclear. It is feasible that a more flexible pocket, such as that found in Mb, may restrict movement of the NO ligand back to the binding site following cleavage of the Fe–N bond, whereas the stiffer Cc pocket does not. The observed photoproduct-binding site following Cc–NO photolysis suggests a well-defined position for the free ligand, whereas the results for Mb do not indicate similar behaviour. A second possibility is that the protein fluctuations may alter the structure of the haem porphyrin in such a way as to restrict rebinding. However, no direct evidence for porphyrin ring involvement in the equilibrium dynamics was observed, suggesting that any effect is likely to be passively controlled by the protein rather than an active effect of the haem.

These results may also relate to the physiological roles of the proteins. It is reasonable to speculate that a ligand transport and storage protein, such as Mb, would require a pocket that does not restrict simple movement of the ligand on and off the binding site, whereas the role played by NO in disrupting the electron transport chain suggests that NO will be likely to bind more permanently to Cc. Indeed, the reported NO off-rate tends to be higher for ferric Mb than for Cc [2], supporting the conclusion that dynamics play a key role in determining biological function.

In conclusion, the results of the present study provide the first insights into the ultrafast equilibrium dynamics of metalloprotein nitrosylation. A combination of 2D-IR and time-resolved IR methods have been applied to study the structural dynamics and geminate rebinding behaviour of NO bound to two ferric haem proteins, Cc and Mb. The data suggest that Cc–NO has a stiffer protein pocket, with reduced equilibrium fluctuations in comparison with Mb. This correlates well with an increased geminate recombination timescale for Mb–NO in comparison with Cc–NO, and indicates an important role for protein fluctuations in determining ligand-binding behaviour in addition to confirming the validity of linear response theories for these systems. Two subsites of ferric Cc–NO are observed, with different vibrational relaxation timescales. These appear to derive from differing interactions between the ligand and the distal Met⁸⁰ residue, although exchange between them was not observed.

AUTHOR CONTRIBUTION

Nicholas Tucker and Neil Hunt conceived the work and prepared the manuscript. Anthony Parker, Neil Hunt, Gregory Greetham and Michael Towrie prepared the ULTRA spectrometer and carried out the spectroscopy. Nicholas Tucker prepared the protein samples and Neil Hunt carried out analysis of the data.

FUNDING

This work was supported by the Engineering and Physical Sciences Research Council (EPSRC) [grant number EP/D071011/1 (to N.T.H.)]; the European Research Council [grant number 202706 (to N.T.H.)]; the STFC (to N.T.H., A.W.P., M.T. and G.M.G.); and the Biotechnology and Biological Sciences Research Council (BBSRC) [grant number FDPG/087 (to A.W.P., M.T. and G.M.G.)]. N.P.T. acknowledges funding from the University of Strathclyde.

REFERENCES

- Brunori, M. (2001) Nitric oxide moves myoglobin centre stage. *Trends Biochem. Sci.* **26**, 209–210
- Cooper, C. E. (1999) Nitric oxide and iron proteins. *Biochim. Biophys. Acta* **1411**, 290–309
- Anfinrud, P. A., Han, C. and Hochstrasser, R. M. (1989) Direct observations of ligand dynamics in hemoglobin by subpicosecond infrared spectroscopy. *Proc. Nat. Acad. Sci. U.S.A.* **86**, 8387–8391
- Kim, S., Jin, G. and Lim, M. (2004) Dynamics of geminate recombination of NO with myoglobin in aqueous solution probed by femtosecond mid-IR spectroscopy. *J. Phys. Chem. B* **108**, 20366–20375
- Carlson, M. L., Regan, R., Elber, R., Haiying, L., Phillips, Jr, G. N., Olson, J. S. and Gibson, Q. H. (1994) Nitric oxide recombination to double mutants of myoglobin: role of ligand diffusion in a fluctuating heme pocket. *Biochemistry* **33**, 10597–10606
- Zemojtel, T., Rini, M., Heyne, K., Dandekar, T., Nibbering, E. T. J. and Kozlowski, P. M. (2004) NO-bound myoglobin: structural diversity and dynamics of the NO ligand. *J. Am. Chem. Soc.* **126**, 1930–1931
- Ye, X., Ionascu, D., Griuia, F., Yu, A., Benabbas, A. and Champion, P. M. (2007) Temperature-dependent heme kinetics with nonexponential binding and barrier relaxation in the absence of protein conformational substates. *Proc. Nat. Acad. Sci. U.S.A.* **104**, 14682–14687
- Ye, X., Yu, A. and Champion, P. M. (2006) Dynamics of nitric oxide rebinding and escape in horseradish peroxidase. *J. Am. Chem. Soc.* **128**, 1444–1445
- Miller, L. M., Pedraza, A. J. and Chance, M. R. (1997) Identification of conformational substates involved in nitric oxide binding to ferric and ferrous myoglobin through difference Fourier transform infrared spectroscopy (FTIR). *Biochemistry* **36**, 12199–12207
- George, S. J., Allen, J. W. A., Ferguson, S. J. and Thorneley, R. N. F. (2000) Time-resolved infrared spectroscopy reveals a stable ferric heme-NO intermediate in the reaction of *Paracoccus pantotrophus* cytochrome cd1 nitrite reductase with nitrite. *J. Biol. Chem.* **275**, 33231–33237
- Merchant, K. A., Noid, W. G., Akiyama, R., Finkelstein, I. J., Goun, A., McClain, B. L., Loring, R. F. and Fayer, M. D. (2003) Myoglobin-CO substate structures and dynamics: multidimensional vibrational echoes and molecular dynamics simulations. *J. Am. Chem. Soc.* **125**, 13804–13818
- Merchant, K. A., Thompson, D. E., Xu, Q. -H., Williams, R. B., Loring, R. F. and Fayer, M. D. (2002) Myoglobin-CO conformational substate dynamics: 2D vibrational echoes and MD simulations. *Biophys. J.* **82**, 3277–3288
- Merchant, K. A., Noid, W. G., Thompson, D. E., Akiyama, R., Loring, R. F. and Fayer, M. D. (2003) Structural assignments and dynamics of the A substates of MbCO: spectrally resolved vibrational echo experiments and molecular dynamics simulations. *J. Phys. Chem. B* **107**, 4–7
- Hochstrasser, R. M. (2007) Two-dimensional spectroscopy at infrared and optical frequencies. *Proc. Nat. Acad. Sci. U.S.A.* **104**, 14190–14196
- Ganim, Z., Chung, H. S., Smith, A. W., Deflores, L. P., Jones, K. C. and Tokmakoff, A. (2008) Amide I two-dimensional infrared spectroscopy of proteins. *Acc. Chem. Res.* **41**, 432–441
- Hunt, N. T. (2009) Ultrafast 2D-IR spectroscopy: applications to biomolecules. *Chem. Soc. Rev.* **38**, 1837–1848
- Ishikawa, H., Kwak, K., Chung, J. K., Kim, S. and Fayer, M. D. (2008) Direct observation of fast protein conformational switching. *Proc. Nat. Acad. Sci. U.S.A.* **105**, 8619–8624
- Ishikawa, H., Kim, S., Kwak, K., Wakasugi, K. and Fayer, M. D. (2007) Disulfide bond influence on protein structural dynamics probed with 2D-IR vibrational echo spectroscopy. *Proc. Nat. Acad. Sci. U.S.A.* **104**, 19309–19314
- Ishikawa, H., Finkelstein, I. J., Kim, S., Kwak, K., Chung, J. K., Wakasugi, K., Massari, A. M. and Fayer, M. D. (2007) Neuroglobin dynamics observed with ultrafast 2D-IR vibrational echo spectroscopy. *Proc. Nat. Acad. Sci. U.S.A.* **104**, 16116–16121
- Finkelstein, I. J., Ishikawa, H., Kim, S., Massari, A. M. and Fayer, M. D. (2007) Substrate binding and protein conformational dynamics measured by 2D-IR vibrational echo spectroscopy. *Proc. Nat. Acad. Sci. U.S.A.* **104**, 2637–2642
- Alderton, W. K., Cooper, C. E. and Knowles, R. G. (2001) Nitric oxide synthases: structure, function and inhibition. *Biochem. J.* **357**, 593–615
- Hill, B. G., Dranka, B. P., Bailey, S. M., Lancaster, Jr, J. R. and Darley-Usmar, V. M. (2010) What part of NO don't you understand? Some answers to the cardinal questions in nitric oxide biology. *J. Biol. Chem.* **285**, 19699–19704
- Justino, M. C., Almeida, C. C., Teixeira, M. and Saraiva, L. M. (2007) *Escherichia coli* di-iron YtfE protein is necessary for the repair of stress-damaged iron-sulfur clusters. *J. Biol. Chem.* **282**, 10352–10359
- Mason, M. G., Holladay, R. S., Nicholls, P., Shepherd, M. and Cooper, C. E. (2008) A quantitative approach to nitric oxide inhibition of terminal oxidases of the respiratory chain. *Methods Enzymol.* **437**, 135–159
- Aono, S. (2008) Metal-containing sensor proteins sensing diatomic gas molecules. *Dalton Trans.* **24**, 3137–3146

- 26 Tucker, N. P., Le Brun, N. E., Dixon, R. and Hutchings, M. I. (2010) There's NO stopping NsrR, a global regulator of the bacterial NO stress response. *Trends Microbiol.* **18**, 149–156
- 27 Benabbas, A., Ye, X., Kubo, M., Zhang, Z. Y., Maes, E. M., Montfort, W. R. and Champion, P. M. (2010) Ultrafast dynamics of diatomic ligand binding to nitrophorin 4. *J. Am. Chem. Soc.* **132**, 2811–2820
- 28 Kubo, M., Gruia, F., Benabbas, A., Barabanschikov, A., Montfort, W. R., Maes, E. M. and Champion, P. M. (2008) Low-frequency mode activity of heme: femtosecond coherence spectroscopy of iron porphyrin halides and nitrophorin. *J. Am. Chem. Soc.* **130**, 9800–9811
- 29 Copeland, D. M., Soares, A. S., West, A. H. and Richter-Addo, G. B. (2006) Crystal structures of the nitrite and nitric oxide complexes of horse heart myoglobin. *J. Inorg. Biochem.* **100**, 1413–1425
- 30 Evans, S. V. and Brayer, G. D. (1990) High-resolution study of the three-dimensional structure of horse heart metmyoglobin. *J. Mol. Biol.* **213**, 885–897
- 31 Bushnell, G. W., Louie, G. V. and Brayer, G. D. (1990) High-resolution three-dimensional structure of horse heart cytochrome c. *J. Mol. Biol.* **214**, 585–595
- 32 Kim, J., Park, J., Lee, T. and Lim, M. (2009) Dynamics of ultrafast rebinding of CO to carboxymethyl cytochrome c. *J. Phys. Chem. B.* **113**, 260–266
- 33 Kania, R., Stewart, A. I., Clark, I. P., Greetham, G. M., Parker, A. W., Towrie, M. and Hunt, N. T. (2010) Investigating the vibrational dynamics of a 17e⁻ metallobonyl intermediate using ultrafast two dimensional infrared spectroscopy. *Phys. Chem. Chem. Phys.* **12**, 1051–1063
- 34 Kwak, K., Park, S., Finkelstein, I. J. and Fayer, M. D. (2007) Frequency–frequency correlation functions and apodization in two-dimensional infrared vibrational echo spectroscopy: a new approach. *J. Chem. Phys.* **127**, 124503
- 35 Roberts, S. T., Loparo, J. J. and Tokmakoff, A. (2006) Characterization of spectral diffusion from two-dimensional line shapes. *J. Chem. Phys.* **125**, 084502
- 36 Park, E. S., Thomas, M. R. and Boxer, S. G. (2000) Vibrational Stark spectroscopy of NO bound to heme: effects of protein electrostatic fields on the NO stretch frequency. *J. Am. Chem. Soc.* **122**, 12297–12303
- 37 Park, S., Kwak, K. and Fayer, M. D. (2007) Ultrafast 2D-IR vibrational echo spectroscopy: a probe of molecular dynamics. *Laser Phys. Lett.* **4**, 704–718
- 38 Kwak, K. and Cho, M. (2003) Two-color pump–probe spectroscopies of two- and three-level systems: 2-dimensional line shapes and solvation dynamics. *J. Phys. Chem. A.* **107**, 5903–5912
- 39 Nutt, D. R. and Meuwly, M. (2007) Ferric and ferrous heme iron in nitroso-myoglobin: computer simulations of stable and metastable states and their infrared spectra. *ChemPhysChem* **8**, 527–536
- 40 Soldatova, A. V., Ibrahim, M., Olson, J. S., Czernuszewicz, R. S. and Spiro, T. G. (2010) New light on NO bonding in Fe(III) heme proteins from resonance Raman spectroscopy and DFT modelling. *J. Am. Chem. Soc.* **132**, 4614–4625
- 41 Kim, S., Chung, J. K., Kwak, K., Bowman, S. E. J., Bren, K. L., Bagchi, B. and Fayer, M. D. (2008) Native and unfolded cytochrome c comparison of dynamics using 2D-IR vibrational echo spectroscopy. *J. Phys. Chem. B* **112**, 10054–10063
- 42 Flynn, P. F., Bieber Urbauer, R. J., Zhang, H., Lee, A. L. and Wand, A. J. (2001) Main chain and side chain dynamics of a heme protein: N-15 and H-2 NMR relaxation studies of *R. capsulatus* ferrocyclochrome c(2). *Biochemistry* **40**, 6559–6569
- 43 Kim, S. and Lim, M. (2005) Protein conformation-induced modulation of ligand binding kinetics: a femtosecond mid-IR study of nitric oxide binding trajectories in myoglobin. *J. Am. Chem. Soc.* **127**, 8908–8909
- 44 Tilton, R. F., Kuntz, I. D. and Petsko, G. A. (1984) Cavities in proteins: structure of a metmyoglobin–xenon complex solved to 1.9 Å. *Biochemistry* **23**, 2849–2857
- 45 Strat, R. M. and Maroncelli, M. (1996) Non-reactive dynamics in solution: the emerging molecular view of solvation dynamics and vibrational relaxation. *J. Phys. Chem.* **100**, 12981–12996
- 46 Geissler, P. L. and Chandler, D. (2000) Importance sampling and theory of nonequilibrium solvation dynamics in water. *J. Chem. Phys.* **113**, 9759
- 47 Tao, G. H. and Strat, R. M. (2006) The molecular origins of nonlinear response in solute energy relaxation: the example of high-energy rotational relaxation. *J. Chem. Phys.* **125**, 114501

Received 15 September 2010/2 November 2010; accepted 11 November 2010

Published as BJ Immediate Publication 11 November 2010, doi:10.1042/BJ20101496